

Postbuckling analysis of functionally graded nanoplates based on nonlocal theory and isogeometric analysis

Son Thai^c, Huu-Tai Thai^{a,b,c,*}, Thuc P. Vo^{d,e}, Seunghye Lee^f

^a*Division of Construction Computation, Institute for Computational Science, Ton Duc Thang University, Ho Chi Minh City, Vietnam*

^b*Faculty of Civil Engineering, Ton Duc Thang University, Ho Chi Minh City, Vietnam*

^c*School of Engineering and Mathematical Sciences, La Trobe University, Bundoora, VIC 3086, Australia*

^d*Institute of Research and Development, Duy Tan University, 03 Quang Trung, Da Nang, Vietnam*

^e*Department of Mechanical and Construction Engineering, Northumbria University, Ellison Place, Newcastle upon Tyne NE1 8ST, UK*

^f*Department of Architectural Engineering, Sejong University 209, Neungdong-ro, Gwangjin-gu, Seoul 05006, Republic of Korea*

Abstract

This study aims to investigate the postbuckling response of functionally graded (FG) nanoplates by using the nonlocal elasticity theory of Eringen to capture the size effect. In addition, Reddy's third-order shear deformation theory is adopted to describe the kinematic relations, while von Kármán's assumptions are used to account for the geometrical nonlinearity. In order to calculate the effective material properties, the Mori-Tanaka scheme is adopted. Governing equations are derived based on the principle of virtual work. Isogeometric analysis (IGA) is employed as a discretization tool, which is able to satisfy the C^1 -continuity demand efficiently. The Newton-Raphson iterative technique with imperfection is employed to trace the postbuckling paths. Various numerical studies are carried out to examine the influences of gradient index, nonlocal effect, ratio of compressive loads, boundary condition, thickness ratio and aspect ratio on the postbuckling behaviour of FG nanoplates.

Keywords: Postbuckling; Nonlocal theory; Functionally graded plates; Isogeometric analysis.

1. Introduction

The use of nanostructures in modern technology is increasingly attracting the attention of many researchers recently owing to their advanced mechanical and electric characteristics [1]. Nanobeams and nanoplates are frequently adopted as fundamental components in biosensors, atomic force microscopes, micro-electro-mechanical systems, nano-electro-mechanical systems. Therefore, a comprehensive understanding of their structural behaviour is needed to be investigated. In fact, the mechanical responses of those small-scale structures are significantly size-dependent as experimentally verified. In order to investigate the behaviour of nanostructures, three common approaches have been

*Corresponding author. E-mail: thaihuutai@tdt.edu.vn (H.T. Thai)

used in the literature: atomistic model [2], hybrid atomistic-continuum mechanic model [3], and non-classical continuum mechanic model [4, 5]. In general, the two former approaches are less popular in practice due to their highly computational cost and complication. In contrast, the non-classical continuum mechanic model is widely employed owing to its simplicity. Based on this model, various theories have been proposed in the literature to capture the size effect in small-scale structures [6]. For nanostructures, the nonlocal elasticity theory [7, 8, 9, 10] is broadly used. According to this theory, the stress at a point of a continuum is assumed to be dependent not only on the strains at that point but also on the strains at other points in the body.

In addition to conventional analyses (e.g. static bending, free vibration, buckling), postbuckling analysis is important for proper design of nanostructures. However, it is seen that there has been only a small number of studies investigating this problem based on the nonlocal elasticity theory in the literature [6]. In a comprehensive study, Shen [11] investigated the nonlinear bending, vibration and postbuckling responses of a stiff thin film resting on an elastic foundation. The author also considered the thermal effect in this study. However, the solutions were only given for simply supported plates. The postbuckling analysis of graphene sheets in a polymer environment was addressed in the work of Naderi and Saidi [12]. The classical plate theory was employed to model the thin graphene sheets subjected to uniaxial and biaxial compressive loads, while the solutions were obtained by using the Galerkin method. By employing the first-order shear deformation theory, Ansari and Gholami [13] examined the buckling and postbuckling behaviour of magneto-electro-thermo nanoplates. In addition, the general differential quadrature method was adopted in their study to obtain the solutions. The buckling and postbuckling responses of piezoelectric nanoplates were also reported by Liu et al. [14]. The authors also adopted the first-order shear deformation theory to describe the kinematic relations, and the solutions were obtained based on the differential quadrature method. Gholami and Ansari [15] proposed a unified high-order shear deformation model to investigate the postbuckling behaviour of rectangular piezoelectric-piezomagnetic nanoplates. Based on the Isogeometric analysis (IGA) approach, Soleimani et al. [16] studied the postbuckling response of orthotropic single-layered graphene sheets under in-plane loadings. The nonlocal plate in this study was also modelled based on the assumptions of first-order shear deformation theory. Overall, it is seen that most of current studies on postbuckling analysis of nanoplates mainly focused on the size effect of graphene sheets, thin films or piezoelectric nanoplates.

In recent years, functionally graded materials (FGMs) appears to be an advanced composite material whose properties vary smoothly in prescribed directions. They have been increasingly used in small scale structures due to their favourable characteristics. [Their application can be found in](#)

various components in high-tech devices such as Micro-electromechanical Systems (MEMS) and Nano-electromechanical Systems (NEMS). FG nanoplates in these devices could be manufactured based on the multilayer process which combines both chemical vapour deposition and high-growth rate plasma-enhanced chemical vapour deposition bulk layer [17]. Although the linear and nonlinear responses of nonlocal FG nanoplates were successfully studied by Natarajan et al. [18], Nguyen et al. [19] and Phung-Van et al. [20], the investigation on their postbuckling behaviour is still limited. Therefore, the main objective of this study is to study the postbuckling response of FG nanoplates based on the nonlocal elasticity theory.

In this study, the Mori-Taknaka scheme [21] is used to calculate the effective material properties of FGMs. The third-order shear deformation theory of Reddy [22] is employed to eliminate the use of shear correction factor. Furthermore, the geometrical nonlinearity is accounted based on the von Kármán's assumptions. The nonlinear governing equations are derived based on the principle of virtual work. The system equation is obtained by employing the IGA approach proposed by Huges et al. [23] as discretization tool, which is able to satisfy the C^1 -continuity requirement of interpolation functions naturally and efficiently [24]. The Newton-Raphson iterative scheme is adopted to trace the postbuckling paths. Geometrical imperfections are imposed to the initial geometry of the plate to obtain the bifurcation buckling paths. Several numerical examples are also presented to find out the influences of gradient index, nonlocal parameter, ratio of in-plane compressive loads, boundary condition, thickness ratio and aspect ratio on the postbuckling response of FG nanoplates.

2. Material descriptions

As described in Fig. 1, a rectangular FGM plate consisting of two distinct materials with their properties varying continuously through the plate thickness is investigated in this study. The top ($z = h/2$) and bottom ($z = -h/2$) surfaces are prescribed ceramic and metal constituents, respectively. Volume fractions of ceramic (V_c) and metal (V_m) constituents at an arbitrary point in the plate's volume are calculated by

$$V_c = \left(\frac{z}{h} + \frac{1}{2} \right)^\kappa ; V_m = 1 - V_c \quad (1)$$

where κ denotes the gradient index.

According to the Mori-Tanaka scheme [21], the effective values of elastic modulus and Poisson's ratio are given by

$$E_e = \frac{9K_e\mu_e}{3K_e + \mu_e} \quad (2)$$

$$\nu_e = \frac{3K_e - 2\mu_e}{2(3K_e + \mu_e)} \quad (3)$$

where K_e and μ_e are the effective bulk and shear modulus, which are defined as follows

$$\frac{K_e - K_m}{K_c - K_m} = \frac{V_c}{1 + V_m \frac{K_c - K_m}{K_m + 4/3\mu_m}} \quad (4)$$

$$\frac{\mu_e - \mu_m}{\mu_c - \mu_m} = \frac{V_c}{1 + V_m \frac{\mu_c - \mu_m}{\mu_m + f_1}} \quad (5)$$

in which $f_1 = \mu_m (9K_m + 8\mu_m) / (6K_m + 2\mu_m)$

3. Nonlocal post-buckling equations

3.1. Overview of nonlocal elasticity theory

According to the nonlocal elasticity theory of Eringen [7, 8, 9, 10], the stress at a point \mathbf{x} in an elastic continuum body is not only calculated based on the strain at its point but also based on the strains at all other points. The nonlocal stress tensor at point \mathbf{x} is given by

$$\boldsymbol{\sigma} = \int_V \zeta(|\mathbf{x}' - \mathbf{x}|, \tau) \mathbf{t}(\mathbf{x}') d\mathbf{x}' \quad (6)$$

where \mathbf{t} is the classical macroscopic stress tensor at point \mathbf{x} . $\zeta(|\mathbf{x}' - \mathbf{x}|, \tau)$ is the kernel function describing the nonlocal modulus. $\tau = e_0 a / \ell$ is a nonlocal parameter describing the nonlocal effect. Herein, e_0 denotes a material constant, a represents an internal characteristic length (e.g. lattice parameter, granular distance, carbon-carbon bond length for graphene sheets), and ℓ is an external characteristic length (e.g. crack length, graphene sheet length, wave length). The classical stress tensor \mathbf{t} relates to the strain tensor according to the Hooke's law as

$$\mathbf{t}(\mathbf{x}) = \mathbf{C}(\mathbf{x}) : \boldsymbol{\varepsilon}(\mathbf{x}) \quad (7)$$

In order to make the integral equation become solvable, Eq. (6) is simplified by applying a linear differential operator $\mathcal{L} = 1 - \mu \nabla^2$ proposed by Eringen [8], where $\mu = (e_0 a)^2$ and ∇^2 is the Laplacian operator. Then, Eq. (6) can be rewritten as

$$(1 - \mu \nabla^2) \boldsymbol{\sigma} = \mathbf{C} : \boldsymbol{\varepsilon} \quad (8)$$

3.2. Kinematic relations and governing equation

By using Reddy's third-order shear deformation theory, the displacement field in Cartesian coordinate system is given by

$$\begin{Bmatrix} u_1 \\ u_2 \\ u_3 \end{Bmatrix} = \begin{Bmatrix} u \\ v \\ w \end{Bmatrix} + f(z) \begin{Bmatrix} \theta_x \\ \theta_y \\ 0 \end{Bmatrix} + g(z) \begin{Bmatrix} -\frac{\partial w}{\partial x} \\ -\frac{\partial w}{\partial y} \\ 0 \end{Bmatrix} \quad (9)$$

where u, v and w denote the displacement components in x, y and z coordinates, θ_x and θ_y are the angular displacements in the middle surface, and $f(z) = z - 4z^3/3h^2$, $g(z) = 4z^3/3h^2$

The strain-displacement relations based on von Kármán's assumptions for large displacements and moderate rotations are given as follows

$$\boldsymbol{\varepsilon}_b = \boldsymbol{\varepsilon}_0 + \frac{1}{2}\boldsymbol{\varepsilon}_{nl} + f(z)\boldsymbol{\varepsilon}_1 + g(z)\boldsymbol{\varepsilon}_2 \quad (10a)$$

$$\boldsymbol{\varepsilon}_s = f'(z)\boldsymbol{\gamma}_1 + (1 - g'(z))\boldsymbol{\gamma}_2 \quad (10b)$$

where

$$\boldsymbol{\varepsilon}_b = \begin{Bmatrix} \varepsilon_{xx} \\ \varepsilon_{yy} \\ \gamma_{xy} \end{Bmatrix}; \boldsymbol{\varepsilon}_0 = \begin{Bmatrix} \frac{\partial u}{\partial x} \\ \frac{\partial v}{\partial y} \\ \frac{\partial u}{\partial y} + \frac{\partial v}{\partial x} \end{Bmatrix}; \boldsymbol{\varepsilon}_{nl} = \begin{Bmatrix} \left(\frac{\partial w}{\partial x}\right)^2 \\ \left(\frac{\partial w}{\partial y}\right)^2 \\ 2\frac{\partial w}{\partial x}\frac{\partial w}{\partial y} \end{Bmatrix}; \boldsymbol{\varepsilon}_1 = \begin{Bmatrix} \frac{\partial \theta_x}{\partial x} \\ \frac{\partial \theta_y}{\partial y} \\ \frac{\partial \theta_x}{\partial y} + \frac{\partial \theta_y}{\partial x} \end{Bmatrix}; \boldsymbol{\varepsilon}_2 = \begin{Bmatrix} -\frac{\partial^2 w}{\partial x^2} \\ -\frac{\partial^2 w}{\partial y^2} \\ -2\frac{\partial^2 w}{\partial x \partial y} \end{Bmatrix} \quad (11a)$$

$$\boldsymbol{\varepsilon}_s = \begin{Bmatrix} \gamma_{xz} \\ \gamma_{yz} \end{Bmatrix}; \boldsymbol{\gamma}_1 = \begin{Bmatrix} \theta_x \\ \theta_y \end{Bmatrix}; \boldsymbol{\gamma}_2 = \begin{Bmatrix} \frac{\partial w}{\partial x} \\ \frac{\partial w}{\partial y} \end{Bmatrix} \quad (11b)$$

The stress resultants defined based on the nonlocal stresses are given by

$$(\mathbf{N}, \mathbf{M}, \mathbf{L}) = \int_{-h/2}^{h/2} \begin{Bmatrix} \sigma_{xx} \\ \sigma_{yy} \\ \sigma_{xy} \end{Bmatrix} (1, f(z), g(z)) dz \quad (12a)$$

$$(\mathbf{T}, \mathbf{U}) = \int_{-h/2}^{h/2} \begin{Bmatrix} \sigma_{xz} \\ \sigma_{yz} \end{Bmatrix} (f'(z), 1 - g'(z)) dz \quad (12b)$$

Then, the constitutive equation expressed in terms of nonlocal stress resultants and strains is given by

$$(1 - \mu \nabla^2) \hat{\boldsymbol{\sigma}} = \hat{\mathbf{D}}_\varepsilon \left(\hat{\boldsymbol{\varepsilon}} + \frac{1}{2} \hat{\boldsymbol{\varepsilon}}_{nl} \right) \quad (13)$$

or in matrix form

$$(1 - \mu \nabla^2) \begin{Bmatrix} \mathbf{N} \\ \mathbf{M} \\ \mathbf{L} \\ \mathbf{T} \\ \mathbf{U} \end{Bmatrix} = \begin{bmatrix} \mathbf{A} & \mathbf{P} & \mathbf{C} & \mathbf{0} & \mathbf{0} \\ \mathbf{P} & \mathbf{H} & \mathbf{F} & \mathbf{0} & \mathbf{0} \\ \mathbf{C} & \mathbf{F} & \mathbf{G} & \mathbf{0} & \mathbf{0} \\ \mathbf{0} & \mathbf{0} & \mathbf{0} & \mathbf{A}_s & \mathbf{P}_s \\ \mathbf{0} & \mathbf{0} & \mathbf{0} & \mathbf{P}_s & \mathbf{C}_s \end{bmatrix} \left(\begin{Bmatrix} \boldsymbol{\varepsilon}_0 \\ \boldsymbol{\varepsilon}_1 \\ \boldsymbol{\varepsilon}_2 \\ \boldsymbol{\gamma}_1 \\ \boldsymbol{\gamma}_2 \end{Bmatrix} + \frac{1}{2} \begin{Bmatrix} \boldsymbol{\varepsilon}_{nl} \\ \mathbf{0} \\ \mathbf{0} \\ \mathbf{0} \\ \mathbf{0} \end{Bmatrix} \right) \quad (14)$$

in which

$$(\mathbf{A}, \mathbf{P}, \mathbf{C}) = \int_{-h/2}^{h/2} (1, f(z), g(z)) \mathbf{Q}_b dz \quad (15a)$$

$$(\mathbf{H}, \mathbf{F}, \mathbf{G}) = \int_{-h/2}^{h/2} ((f(z))^2, f(z)g(z), (g(z))^2) \mathbf{Q}_b dz \quad (15b)$$

$$(\mathbf{A}_s, \mathbf{P}_s, \mathbf{C}_s) = \int_{-h/2}^{h/2} ((f'(z))^2, (f'(z))(1-g'(z)), (1-g'(z))^2) \mathbf{Q}_s dz \quad (15c)$$

For FGMs, \mathbf{Q}_b and \mathbf{Q}_s are given as follows

$$\mathbf{Q}_b = \frac{E(z)}{1 - [\nu(z)]^2} \begin{bmatrix} 1 & \nu(z) & 0 \\ \nu(z) & 1 & 0 \\ 0 & 0 & (1 - \nu(z))/2 \end{bmatrix}; \mathbf{Q}_s = \frac{E(z)}{(1 + \nu(z))} \begin{bmatrix} 1 & 0 \\ 0 & 1 \end{bmatrix} \quad (16)$$

According to the elasticity theory, the virtual strain gradient and the virtual work of external distributed traction force and boundary traction force are given as follows

$$\delta U = \int_V \sigma_{ij} \delta \varepsilon_{ij} dV = \int_V \delta \boldsymbol{\varepsilon}^T \boldsymbol{\sigma} dV \quad (17a)$$

$$\delta W_f = - \int_{\Omega} \hat{f}_i \delta u_i d\Omega = - \int_{\Omega} \delta \mathbf{u}_f^T \hat{\mathbf{f}} d\Omega \quad (17b)$$

$$\delta W_t = - \int_S \hat{t}_i \delta u_i dS = - \int_S \delta \mathbf{u}_t^T \hat{\mathbf{t}} dS \quad (17c)$$

where Ω denotes the domain of middle plate, S is the boundary where the traction force $\hat{\mathbf{t}}$ is applied, $\hat{\mathbf{f}}$ is the surface distributed traction load, \mathbf{u}_t and \mathbf{u}_f are the corresponding degrees of freedom for each loading cases, respectively.

To consider the nonlocal effect, the differential operator $\mathcal{L} = 1 - \mu \nabla^2$ is multiplied to the equation of principle of virtual work $\delta U + \delta W = 0$. In addition, by adopting an assumption that the strains are small, the governing equation for postbuckling problems of nonlocal plates derived from the principle of virtual work can be expressed with respect to the initial configuration for the cases of surface distributed traction force and boundary traction force as follows

$$\int_{\Omega} \delta \left(\hat{\boldsymbol{\varepsilon}} + \frac{1}{2} \boldsymbol{\varepsilon}_{nl} \right)^T \hat{\mathbf{D}}_{\boldsymbol{\varepsilon}} \left(\hat{\boldsymbol{\varepsilon}} + \frac{1}{2} \boldsymbol{\varepsilon}_{nl} \right) d\Omega = \int_{\Omega} \delta \mathbf{u}^T (1 - \mu \nabla^2) \hat{\mathbf{f}} d\Omega \quad (18)$$

$$\int_{\Omega} \delta \left(\hat{\boldsymbol{\varepsilon}} + \frac{1}{2} \boldsymbol{\varepsilon}_{nl} \right)^T \hat{\mathbf{D}}_{\boldsymbol{\varepsilon}} \left(\hat{\boldsymbol{\varepsilon}} + \frac{1}{2} \boldsymbol{\varepsilon}_{nl} \right) d\Omega = \int_S \left(\delta \mathbf{u}^T - \mu \frac{d\delta \mathbf{u}^T}{dS^2} \right) \hat{\mathbf{t}} dS \quad (19)$$

4. IGA-based finite element formulations

According to the IGA approach, the middle domain Ω of a rectangular plate can be expressed as a b-spline surface

$$\Omega(x, y) = \sum_{i=1}^n \sum_{j=1}^m R_{i,j}^{p,q}(\xi, \eta) \mathbf{B}_{i,j} \quad (20)$$

where $H_{i,j}^{p,q}(\xi, \eta)$ are the 2-dimensional b-spline basis functions and $\mathbf{B}_{i,j}$ is the control net. The b-spline basis functions are constructed based on a tensor product of two univariate b-spline basis functions as

$$R_{i,j}^{p,q}(\xi, \eta) = \sum_{i=1}^n \sum_{j=1}^m N_{i,p}(\xi) M_{j,q}(\eta) \quad (21)$$

in which, $N_{i,p}(\xi)$ and $M_{j,q}(\eta)$ are the basis functions in ξ and η directions. These two basis functions are defined based on two knot vectors $\Xi = \{\xi_1, \xi_2, \xi_3, \dots, \xi_{n+p+1}\}$ and $\Psi = \{\eta_1, \eta_2, \eta_3, \dots, \eta_{n+q+1}\}$ according to the Cox-de Boor recursion formula as follows. For $p = 0$

$$N_{i,0}(\xi) = \begin{cases} 1 & \xi_i \leq \xi < \xi_{i+1} \\ 0 & \text{otherwise} \end{cases} \quad (22)$$

and for $p \geq 1$

$$N_{i,p} = \frac{\xi - \xi_i}{\xi_{i+p} - \xi_i} N_{i,p-1}(\xi) + \frac{\xi_{i+p+1} - \xi}{\xi_{i+p+1} - \xi_{i+1}} N_{i+1,p-1}(\xi) \quad (23)$$

More details of b-spline basis functions, IGA techniques and implementations could be found in [23, 25].

In this study, the IGA approach is employed to discretize the governing equation presented in Eq. (19). The displacement variables are approximated by using the b-spline basis function as

$$\mathbf{u} = \sum_{c=1}^{ncp} R_c \mathbf{d}_c \quad (24)$$

where ncp denotes the number of control points in an element, $\mathbf{u} = \left\{ u \ v \ \theta_x \ \theta_y \ w \right\}^T$, and $\mathbf{d}_c = \left\{ u \ v \ \theta_x \ \theta_y \ w \right\}_c^T$ is the degrees of freedom associated with a control point.

Substitute Eq. (24) into Eq. (11), the strains are interpolated as follows

$$\begin{pmatrix} \varepsilon_0 \\ \varepsilon_1 \\ \varepsilon_2 \\ \gamma_1 \\ \gamma_2 \end{pmatrix} = \sum_c^{ncp} \begin{pmatrix} \mathbf{B}_0 \\ \mathbf{B}_1 \\ \mathbf{B}_2 \\ \mathbf{B}_3 \\ \mathbf{B}_4 \end{pmatrix}_c \mathbf{d}_c \quad (25a)$$

$$\varepsilon_{nl} = \sum_c^{ncp} \mathbf{B}_{nlc} \mathbf{d}_c = \sum_c^{ncp} \Lambda \mathbf{B}_{gc} \mathbf{d}_c \quad (25b)$$

where

$$\mathbf{B}_0 = \begin{bmatrix} \frac{\partial R}{\partial x} & 0 & 0 & 0 & 0 \\ 0 & \frac{\partial R}{\partial y} & 0 & 0 & 0 \\ \frac{\partial R}{\partial y} & \frac{\partial R}{\partial x} & 0 & 0 & 0 \end{bmatrix} \quad (26a)$$

$$\mathbf{B}_1 = \begin{bmatrix} 0 & 0 & \frac{\partial R}{\partial x} & 0 & 0 \\ 0 & 0 & 0 & \frac{\partial R}{\partial y} & 0 \\ 0 & 0 & \frac{\partial R}{\partial y} & \frac{\partial R}{\partial x} & 0 \end{bmatrix} \quad (26b)$$

$$\mathbf{B}_2 = \begin{bmatrix} 0 & 0 & 0 & 0 & -\frac{\partial^2 R}{\partial x^2} \\ 0 & 0 & 0 & 0 & -\frac{\partial^2 R}{\partial y^2} \\ 0 & 0 & 0 & 0 & -2\frac{\partial^2 R}{\partial x \partial y} \end{bmatrix} \quad (26c)$$

$$\mathbf{B}_3 = \begin{bmatrix} 0 & 0 & R_c & 0 & 0 \\ 0 & 0 & 0 & R_c & 0 \end{bmatrix} \quad (26d)$$

$$\mathbf{B}_4 = \begin{bmatrix} 0 & 0 & 0 & 0 & \frac{\partial R}{\partial x} \\ 0 & 0 & 0 & 0 & \frac{\partial R}{\partial y} \end{bmatrix} \quad (26e)$$

$$\mathbf{\Lambda} = \begin{bmatrix} \frac{\partial w}{\partial x} & 0 \\ 0 & \frac{\partial w}{\partial y} \\ \frac{\partial w}{\partial y} & \frac{\partial w}{\partial x} \end{bmatrix} \quad (26f)$$

$$\mathbf{B}_g = \begin{bmatrix} 0 & 0 & 0 & 0 & \frac{\partial R}{\partial x} \\ 0 & 0 & 0 & 0 & \frac{\partial R}{\partial y} \end{bmatrix} \quad (26g)$$

In the next step, the system equation is obtained by using Eq. (25) in Eq. (19) as follows

$$\mathbf{Kd} = \mathbf{f} \quad (27)$$

where \mathbf{K} is the stiffness matrix, \mathbf{f} is the load vector of either surface distributed traction load ($\mathbf{f} = \mathbf{f}_f$) or boundary traction load ($\mathbf{f} = \mathbf{f}_t$).

$$\mathbf{K} = \int_{\Omega} (\mathbf{B}_{LT} + \mathbf{B}_{NLT})^T \hat{\mathbf{D}} \left(\mathbf{B}_L + \frac{1}{2} \mathbf{B}_{NL} \right) d\Omega \quad (28a)$$

$$\mathbf{f}_f = \int_S (\mathbf{B}_{f1} - \mu \mathbf{B}_{f2})^T \hat{\mathbf{f}} dS \quad (28b)$$

$$\mathbf{f}_t = \int_S (\mathbf{N}_1 - \mu \mathbf{N}_2)^T \hat{\mathbf{t}} dS \quad (28c)$$

where

$$\mathbf{B}_L = \begin{Bmatrix} \mathbf{B}_0 \\ \mathbf{B}_1 \\ \mathbf{B}_2 \\ \mathbf{B}_3 \\ \mathbf{B}_4 \end{Bmatrix}; \mathbf{B}_{LT} = \begin{Bmatrix} \mathbf{B}_0^T \\ \mathbf{B}_1^T \\ \mathbf{B}_2^T \\ \mathbf{B}_3^T \\ \mathbf{B}_4^T \end{Bmatrix}; \mathbf{B}_{NL} = \begin{Bmatrix} \mathbf{B}_{nl} \\ \mathbf{0} \\ \mathbf{0} \\ \mathbf{0} \\ \mathbf{0} \end{Bmatrix}; \mathbf{B}_{NLT} = \begin{Bmatrix} \mathbf{B}_{nl}^T \\ \mathbf{0} \\ \mathbf{0} \\ \mathbf{0} \\ \mathbf{0} \end{Bmatrix} \quad (29a)$$

$$\mathbf{B}_{f1} = \begin{bmatrix} 0 & 0 & 0 & 0 & R \end{bmatrix} \quad (29b)$$

$$\mathbf{B}_{f2} = \begin{bmatrix} 0 & 0 & 0 & 0 & \frac{\partial^2 R}{\partial x^2} + \frac{\partial^2 R}{\partial y^2} \end{bmatrix} \quad (29c)$$

$$\mathbf{N}_1 = \begin{bmatrix} N & N & 0 & 0 & 0 \end{bmatrix} \quad (29d)$$

$$\mathbf{N}_2 = \begin{bmatrix} \frac{\partial^2 N}{\partial S^2} & \frac{\partial^2 N}{\partial S^2} & 0 & 0 & 0 \end{bmatrix} \quad (29e)$$

where N are 1-dimensional basis functions defined along the boundary S . As can be seen in Eqs. (26) and (29), the interpolation functions having C^1 -continuity over the element boundaries should be given to construct the stiffness matrix and force vector. In the IGA approach, this requirement is met efficiently and naturally due to the advanced features of b-spline basis functions and the unique k -refinement procedure [24].

To solve the nonlinear equation as given in Eq. (27), the Newton-Raphson iterative technique is employed in this study. It should be noted that the bifurcation buckling phenomenon could be obtained when the postbuckling problem is solved on the basis of geometrically nonlinear analysis, in which a small initial geometrical imperfection is imposed to the initial geometry of the plate [26]. [Herein, the initial imperfection is the fundamental deformed shape obtained from the linear buckling analysis with the magnitude of imperfection being \$0.001h\$. This value is chosen to be relatively small so that it does not affect the postbuckling behaviour significantly and the computational problems can be avoided.](#) The tangent stiffness matrix of the present model is computed as follows

$$\mathbf{T} = \frac{\partial \mathbf{K}}{\partial \mathbf{d}} \mathbf{d} + \mathbf{K} = \mathbf{K}_L + \mathbf{K}_{NL} + \mathbf{K}_\sigma \quad (30)$$

where

$$\mathbf{K}_L = \int_{\Omega} \mathbf{B}_{LT}^T \hat{\mathbf{D}} \mathbf{B}_L d\Omega \quad (31a)$$

$$\mathbf{K}_{NL} = \int_{\Omega} \left(\mathbf{B}_{LT}^T \hat{\mathbf{D}} \mathbf{B}_{NL} + \mathbf{B}_{NLT}^T \hat{\mathbf{D}} \mathbf{B}_L + \mathbf{B}_{NLT}^T \hat{\mathbf{D}} \mathbf{B}_{NL} \right) d\Omega \quad (31b)$$

$$\mathbf{K}_\sigma = \int_{\Omega} \mathbf{B}_g^T \hat{\mathbf{N}} \mathbf{B}_g d\Omega \quad (31c)$$

$$\hat{\mathbf{N}} = \begin{bmatrix} N_x & N_{xy} \\ N_{xy} & N_y \end{bmatrix} \quad (31d)$$

5. Numerical examples

5.1. Verification and convergence studies

To the best of the authors' knowledge, there is no study on the postbuckling of FG nanoplates. Therefore, a postbuckling problem of an armchair graphene sheet addressed in the study of Naderi and Saidi [12] is revisited to verify the reliability and accuracy of the present approach. Material properties and geometrical information of the armchair graphene sheet are listed as follows: $E_{11} = 1949$ GPa, $E_{22} = 1962$ GPa, $\nu_{12} = 0.201$, $G_{12} = 846$ GPa, $a \times b = 4.888 \times 4.855$ nm², and $h = 0.156$ nm, and the values of nonlocal parameter is $e_0 a = 0.27$ nm, which was obtained from the molecular dynamics simulation [27]. Herein, the shear modulus are assumed to be $G_{13} = G_{23} = G_{12}$. The simply supported boundary condition (SSSS1) is employed in this example with

$$w = 0 \text{ at } y = 0 \text{ and } y = b, x = 0 \text{ and } x = a \quad (32)$$

Fig. 2 compares the postbuckling paths obtained by Naderi and Saidi [12] and present study with different mesh sizes. Herein, B-spline basis functions with $p = q = 3$ are employed for a better convergence rate. As can be seen from Fig. 2, the obtained results from the present approach and those provided in the referenced study are in good agreement. In addition, it is seen that a mesh of 12×12 is sufficient to obtain the accurate results, hence this mesh size is used in the remaining calculations. The difference between the present results and those from previous study in the latter part of postbukling paths is due to the shear deformation effect, which is not accounted in Naderi and Saidi [12].

To further verify the ability of the present model, a geometrically nonlinear bending problem of a FG nanoplate presented by Phung-Van et al. [20] is resolved. The square plate has a length dimension of $a = 10$ and a thickness ratio of $a/h = 10$ nm, it is made of Al/ZnO₂ where $E_c = 151$ GPa, $E_m = 70$ GPa, and $\nu_c = \nu_m = 0.3$. The simply supported boundary condition (SSSS2) of the plate in this example is given as follows

$$u = \theta_x = w = 0 \text{ at } y = 0 \text{ and } y = b \quad (33a)$$

$$v = \theta_y = w = 0 \text{ at } x = 0 \text{ and } x = a \quad (33b)$$

As can be seen in Fig. 3, the results obtained from the present model agree well with those given by Phung-Van et al. [20]. When the nonlocal parameter μ increases, the nonlocal effect becomes more considerable and larger deflections are obtained.

5.2. Parametric investigations and discussions

This subsection is dedicated to figure out the influences of different input information, such as gradient index κ , nonlocal parameter e_0a , ratio of compression loads $\lambda = N_y/N_x$, boundary conditions, thickness ratio h/a , and aspect ratio a/b , on the postbuckling response of FG nanoplates. The ceramic and metal constituents are chosen to be Si3N4 and Al, where $E_c = 384.43$ GPa, $E_m = 70$ GPa, and $\nu_c = \nu_m = 0.3$, respectively. **In addition, the length of rectangular nanoplates is assumed to be $a = 17$ nm. The remaining dimensions of width and thickness are defined based on the thickness and aspect ratios.** The nonlocal parameter is assumed to be $e_0a \leq 2$ nm [28]. For convenience purpose, a normalized quantity is introduced, where $\bar{N}_x = N_x a^2 / E_m h^3$. Two more boundary conditions, which are prescribed as follows, are also taken into investigation in this subsection

- CCCC1

$$\theta_x = \theta_y = w = \frac{\partial w}{\partial y} = 0 \text{ at } y = 0 \text{ and } y = b \quad (34a)$$

$$\theta_x = \theta_y = w = \frac{\partial w}{\partial x} = 0 \text{ at } x = 0 \text{ and } x = a \quad (34b)$$

- CCCC2

$$u = \theta_x = \theta_y = w = \frac{\partial w}{\partial y} = 0 \text{ at } y = 0 \text{ and } y = b \quad (35a)$$

$$v = \theta_x = \theta_y = w = \frac{\partial w}{\partial x} = 0 \text{ at } x = 0 \text{ and } x = a \quad (35b)$$

In the first investigation, the influence of gradient index κ on the postbuckling response is examined. The square plate ($h/a = 0.05$) is subjected to uniaxial compressive loads, the nonlocal parameter in this case is $e_0a = 0.15$ nm, and the simply supported (SSSS2) boundary condition is considered. As depicted in Fig. 4, the postbuckling paths obtained from different gradient indices are different to each other. By increasing the gradient index κ , the postbuckling parts are lowered, which means the plate having greater κ value would deform lager with the same amount of compressive loads. This phenomenon is easy to understand since the greater the gradient index is, the more metal constituent the plate has, and a weaker plate is given accordingly. In addition, it is worth noticing that the bifurcation postbuckling is obtained only when the plate is homogeneous ($\kappa = 0$). In other cases where the material throughout the thickness is graded, the plate deforms as soon as the compressive loads are applied. This is owing to the coupling stress resultants induced by the difference between midplane and physical neutral plane.

In Fig. 5, the postbuckling paths obtained from different nonlocal parameters are illustrated. The plate in this case is assumed to be square, $h/a = 0.05$, and subjected to uniaxial compressive loads. In addition, two material models ($\kappa = 0$ and $\kappa = 2$) are investigated. As can be seen from the figures,

the load-bearing capacity of nanoplate is reduced with the increment of nonlocal parameter e_0a . In other words, the nonlocal effect tends to reduce the stiffness of the plate in nano-scale when it is subjected to in-plane compressive loads. The postbuckling paths obtained from homogeneous and inhomogeneous plates are distinguishable due to the coupling effect as discussed earlier. In case of homogeneous plate ($\kappa = 0$), the postbuckling paths with $e_0a = 0$ and $e_0a = 0.1$ are almost identical. However, a difference between those cases can be recognized when the inhomogeneous plate ($\kappa = 2$) is considered. For other cases, it is seen that the effect of nonlocal parameter is not similar and changes to different degrees when material properties are varied. This is shown by the distance between post buckling paths in Figs. 5a and 5b.

The influence of ratio of compressive loads $\lambda = N_y/N_x$ on the postbuckling behaviour of FG nanoplates is depicted in Fig. 6. In general, the buckling load decreases when the ratio λ is elevated in both cases of homogeneous and inhomogeneous plates ($\kappa = 0$ and $\kappa = 2$). In addition, it is observed that the rate of decrease of buckling load reduces with λ . In Fig. 7, the influence of boundary conditions is illustrated. It is seen that the plates having clamped boundary conditions (CCCC1 and CCCC2) have much greater buckling loads compared to those with simply supported boundaries. This is due to the fact that the clamped boundaries are able to prevent the plate from deforming under initial coupling stress resultants. Having more constrained degrees of freedom, the plates with additional in-plane constraints (SSSS2, CCCC2) exhibit smaller displacements compared to those whose all edges are free to move (SSSS1 and CCCC1). [The influence of thickness ratio \(\$h/a\$ \) is presented in Fig. 8. When the thickness is relatively small compared to the length of the plate \(\$h/a = 0.01, 0.02, 0.05\$ \), the obtained results are almost identical as the shear deformation effect is small and can be neglected. However, this effect becomes considerable when thicker plates \(\$h/a = 0.1, 0.2\$ \) are investigated as indicated in Fig. 8.](#)

Finally, the influence of aspect ratio (a/b) on the postbuckling response of FG nanoplates is investigated. In Fig. 9, the postbuckling paths of different rectangular FG nanoplates under the effect of uniaxial compressive loads N_x are illustrated. It is seen that the aspect ratio a/b has a noticeable influence on the post buckling response of FG nanoplates. The rise of aspect ratio (a/b) leads to an increase in buckling load. In other words, when the edges subjected to compressive loads are shorten, the compressive loads (force/unit of length) need to be increased to make the plate deform the same amount as the cases having longer edges. It is worth noting that the uniaxial compressive loads are applied along the edges $y = 0, b$. Furthermore, it should be noted that when the aspect ratio (a/b) is changed, the geometrical imperfection imposed to the initial geometry of homogeneous plates is changed (e.g. when $a/b = 0.5, 1$, the number of wave-length in the fundamental linear

buckling shape is 1, the corresponding numbers for the cases of $a/b = 1.5, 2$ and $a/b = 2.5, 3$ are 2 and 3, respectively). On the other hand, the postbuckling response of FG plates ($\kappa \neq 0$) do not depend on the initial imperfection as the plates deform immediately when the compressive loads are imposed. For illustration purpose, the deformed geometries obtained from postbuckling analysis of homogeneous ($\kappa = 0$, bifurcation buckling) and inhomogeneous ($\kappa = 2$) plates [having SSSS1 boundary conditions](#) are presented with adopted scale factors in Figs. 10 and 11. It is seen that the deformed geometry of FG plate is different to that of homogeneous plate when $a/b = 1.5$.

6. Conclusions

In this paper, the postbuckling behaviour of FG nanoplates is investigated based on the IGA approach. The nonlocal elasticity theory is adopted to capture the size effect. The Mori-Tanaka scheme is used to evaluate the effective properties of FGMs. The kinematic relations are based on the third-order shear deformation theory, and von Kármán's assumptions are used to account for the geometrical nonlinearity. The governing equations are derived based on the principle of virtual work. The discretization procedure is implemented on the basis of the IGA approach, where the b-spline basis functions are used as interpolation functions to satisfy the C^1 -continuity demand. The postbuckling paths are traced by using the Newton-Raphson iterative scheme. Initial geometrical imperfections obtained from linear buckling analysis are used in the iterative scheme to capture the bifurcation buckling phenomenon of homogeneous plates. The accuracy of the present approach is verified by comparing the obtained results with those available in the literature. In addition, various parametric investigations are carried out to study the influences of gradient index, nonlocal parameter, ratio of compressive loads, boundary condition, thickness ratio and aspect ratio on the postbuckling response of FG nanoplate. Finally, the paper is closed with some specific remarks as follows:

- Larger postbuckling deformations are obtained with greater gradient indices as the consequence of the increase of volume fraction of the weaker material in the plate's volume.
- The nonlocal elasticity theory has a noticeable influence on the postbuckling behaviour of nanoplates. The increase of nonlocal parameter leads to a reduction of the buckling loads.
- The bifurcation postbuckling phenomenon is always obtained regardless of the material properties when the clamped boundary conditions are considered, whereas this phenomenon in simply supported plates is only obtained when a homogeneous material is considered.
- The influence of aspect ratios is worth noticing. It is observed that the deformed geometries obtained from homogeneous plates and FG plates are different to each other in some cases.

Acknowledgements

This research study was supported by La Trobe University under its Disciplinary Research Program (DRP) and Postgraduate Research Scholarship. This financial support is gratefully acknowledged

References

- [1] Li X, Bhushan B, Takashima K, Baek CW, Kim YK. Mechanical characterization of micro/nanoscale structures for MEMS/NEMS applications using nanoindentation techniques. *Ultramicroscopy* 2003;97(1):481–494.
- [2] Baughman RH, Zakhidov AA, Heer WAd. Carbon Nanotubes—the Route Toward Applications. *Science* 2002;297(5582):787–792.
- [3] Li C, Chou TW. Single-walled carbon nanotubes as ultrahigh frequency nanomechanical resonators. *Physical Review B* 2003;68(7):073405.
- [4] Wang CM, Tan VBC, Zhang YY. Timoshenko beam model for vibration analysis of multi-walled carbon nanotubes. *Journal of Sound and Vibration* 2006;294(4):1060–1072.
- [5] Reddy JN. Nonlocal nonlinear formulations for bending of classical and shear deformation theories of beams and plates. *International Journal of Engineering Science* 2010;48(11):1507–1518.
- [6] Thai HT, Vo TP, Nguyen TK, Kim SE. A review of continuum mechanics models for size-dependent analysis of beams and plates. *Composite Structures* 2017;177:196–219.
- [7] Eringen, Cemal A. *Nonlocal Continuum Field Theories*. Springer-Verlag New York , 2002.
- [8] Eringen AC. Nonlocal polar elastic continua. *Int J Eng Sci* 1972;10(1):1–16.
- [9] Eringen A, Edelen D. On nonlocal elasticity. *International Journal of Engineering Science* 1972;10(3):233–248. Cited By 818.
- [10] Eringen AC. On differential equations of nonlocal elasticity and solutions of screw dislocation and surface waves. *J Appl Phys* 1983;54(9):4703.
- [11] Shen HS. Nonlocal plate model for nonlinear analysis of thin films on elastic foundations in thermal environments. *Composite Structures* 2011;93(3):1143–1152.

- [12] Naderi A, Saidi AR. Nonlocal postbuckling analysis of graphene sheets in a nonlinear polymer medium. *International Journal of Engineering Science* 2014;81:49–65.
- [13] Ansari R, Gholami R. Size-Dependent Buckling and Postbuckling Analyses of First-Order Shear Deformable Magneto-Electro-Thermo Elastic Nanoplates Based on the Nonlocal Elasticity Theory. *International Journal of Structural Stability and Dynamics* 2016;17(01):1750014.
- [14] Liu C, Ke LL, Yang J, Kitipornchai S, Wang YS. Buckling and post-buckling analyses of size-dependent piezoelectric nanoplates. *Theoretical and Applied Mechanics Letters* 2016;6(6):253–267.
- [15] Gholami R, Ansari R. A unified nonlocal nonlinear higher-order shear deformable plate model for postbuckling analysis of piezoelectric-piezomagnetic rectangular nanoplates with various edge supports. *Composite Structures* 2017;166:202–218.
- [16] Soleimani A, Naei MH, Mashhadi MM. Nonlocal postbuckling analysis of graphene sheets with initial imperfection based on first order shear deformation theory. *Results in Physics* 2017;7:1299–1307.
- [17] Witvrouw A, Mehta A. The Use of Functionally Graded Poly-SiGe Layers for MEMS Applications. *Materials Science Forum* 2005;492-493:255–260.
- [18] Natarajan S, Chakraborty S, Thangavel M, Bordas S, Rabczuk T. Size-dependent free flexural vibration behavior of functionally graded nanoplates. *Computational Materials Science* 2012;65:74–80.
- [19] Nguyen NT, Hui D, Lee J, Nguyen-Xuan H. An efficient computational approach for size-dependent analysis of functionally graded nanoplates. *Computer Methods in Applied Mechanics and Engineering* 2015;297:191–218.
- [20] Phung-Van P, Ferreira AJM, Nguyen-Xuan H, Abdel Wahab M. An isogeometric approach for size-dependent geometrically nonlinear transient analysis of functionally graded nanoplates. *Composites Part B: Engineering* 2017;118:125–134.
- [21] Mori T, Tanaka K. Average stress in matrix and average elastic energy of materials with misfitting inclusions. *Acta Metallurgica* 1973;21(5):571–574.
- [22] Reddy JN. A Simple Higher-Order Theory for Laminated Composite Plates. *Journal of Applied Mechanics* 1984;51(4):745–752.

- [23] Hughes TJR, Cottrell JA, Bazilevs Y. Isogeometric analysis: CAD, finite elements, NURBS, exact geometry and mesh refinement. *Computer Methods in Applied Mechanics and Engineering* 2005;194(3941):4135–4195.
- [24] Nguyen VP, Anitescu C, Bordas SPA, Rabczuk T. Isogeometric analysis: An overview and computer implementation aspects. *Mathematics and Computers in Simulation* 2015;117:89–116.
- [25] Cottrell JA, Hughes TJR, Bazilevs Y. *Isogeometric Analysis: Toward Integration of CAD and FEA*. 1st ed. , Wiley Publishing , 2009.
- [26] Le-Manh T, Lee J. Postbuckling of laminated composite plates using NURBS-based isogeometric analysis. *Composite Structures* 2014;109:286–293.
- [27] Shen L, Shen HS, Zhang CL. Nonlocal plate model for nonlinear vibration of single layer graphene sheets in thermal environments. *Computational Materials Science* 2010;48(3):680–685.
- [28] Wang Q, Wang CM. The constitutive relation and small scale parameter of nonlocal continuum mechanics for modelling carbon nanotubes. *Nanotechnology* 2007;18(7):075702.

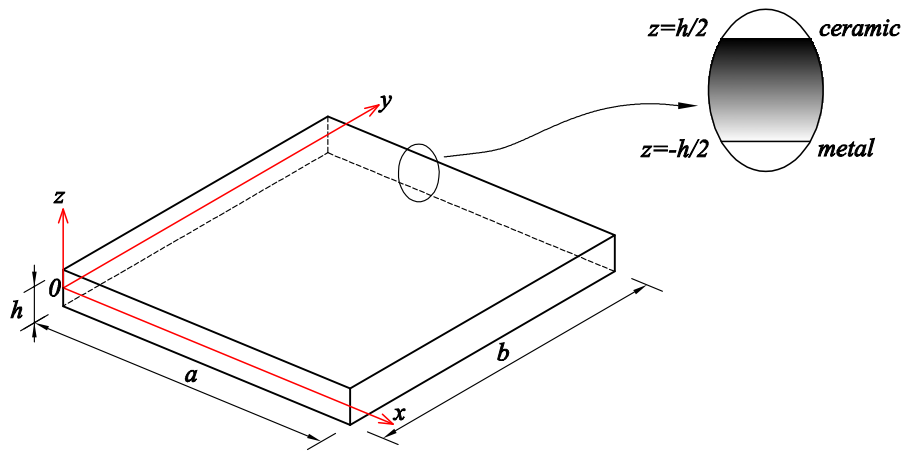


Figure 1: Configuration and coordinate system of a rectangular FG nanoplate

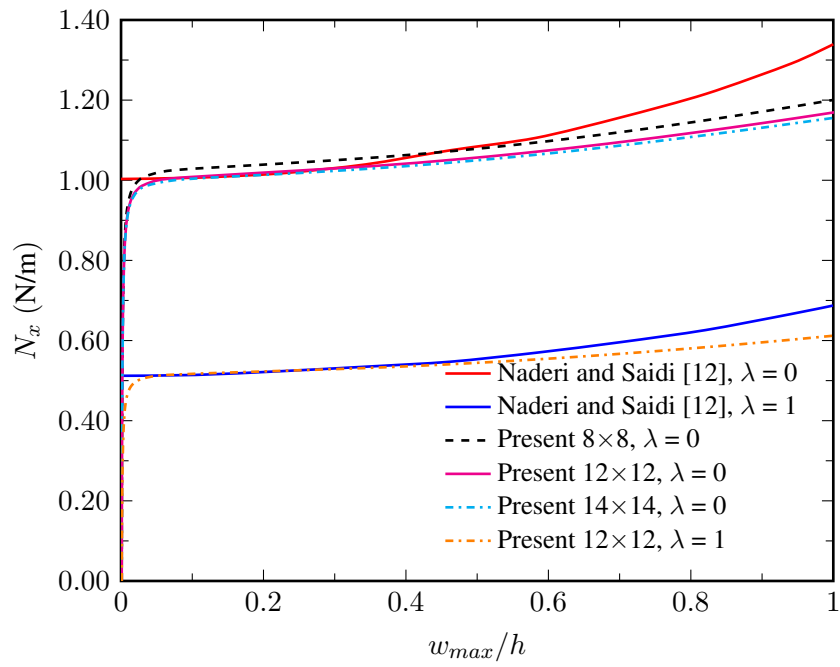


Figure 2: Postbuckling paths of an armchair graphene sheet ($\lambda = N_y/N_x$)

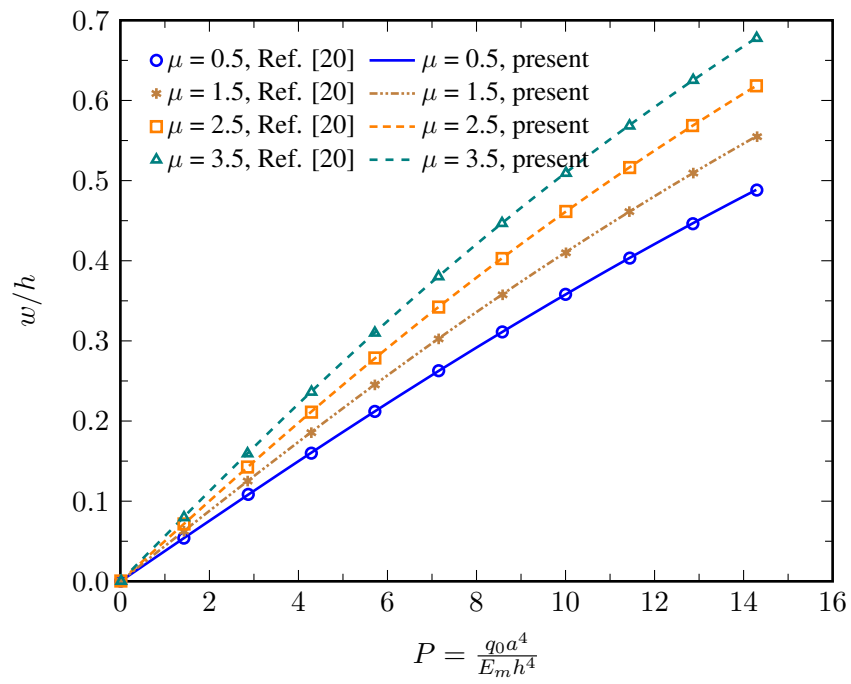


Figure 3: Geometrically nonlinear bending behaviour of SSSS2 FG nanoplate ($\kappa=2$)

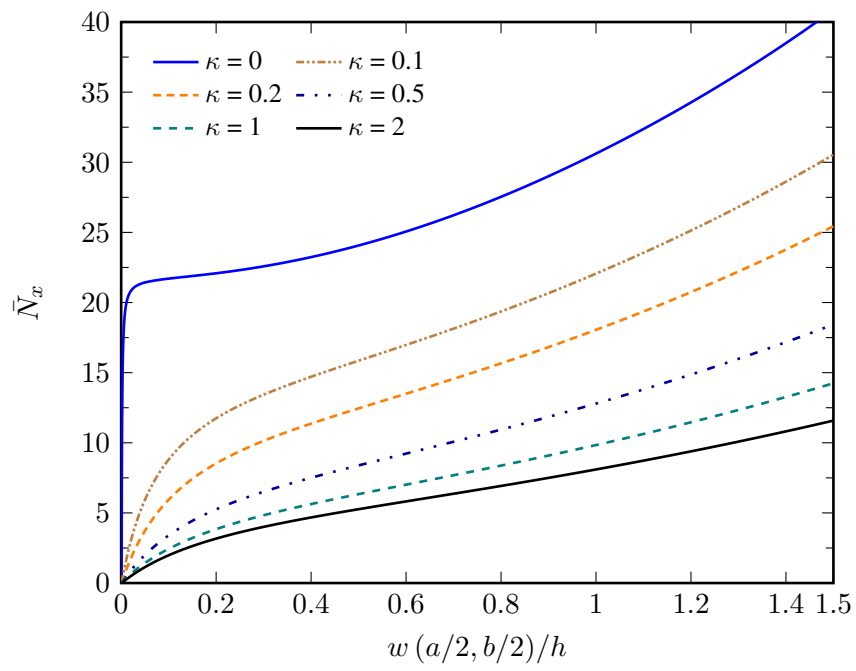
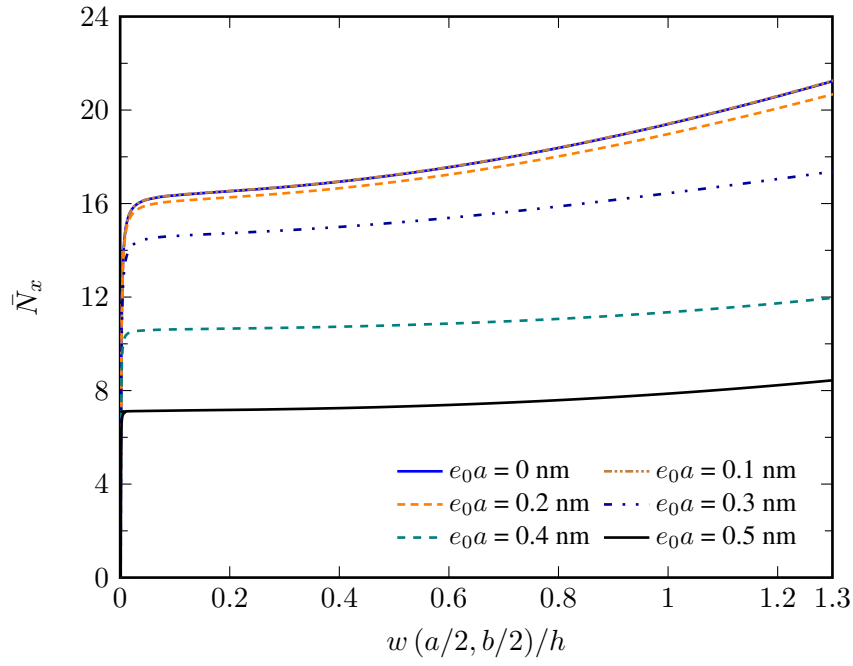
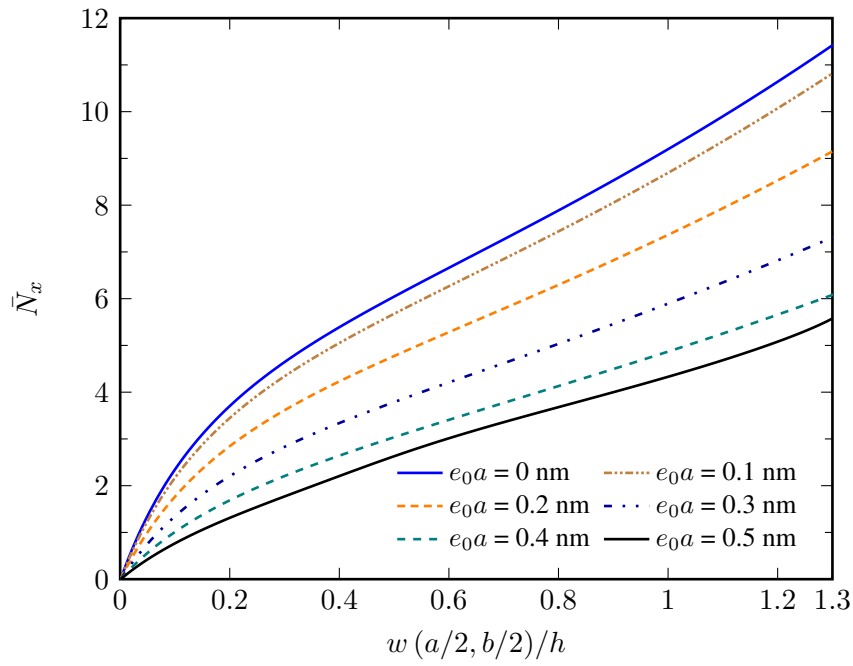


Figure 4: Influence of gradient index κ on postbuckling paths of square FGM SSSS2 nanoplate ($\lambda = 0$, $e_0 a = 0.15$ nm, $h/a = 0.05$)

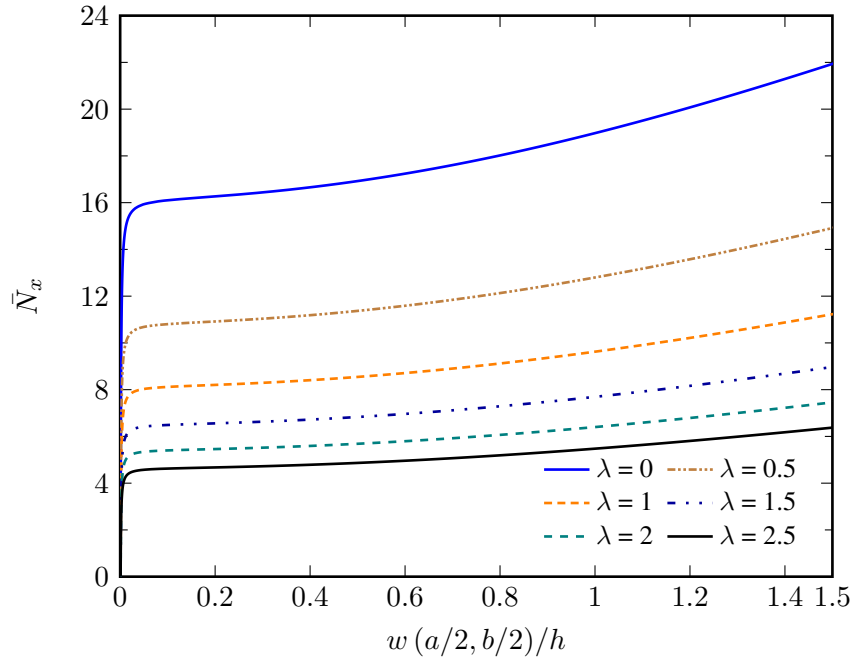


(a) SSSS1, $\kappa = 0$

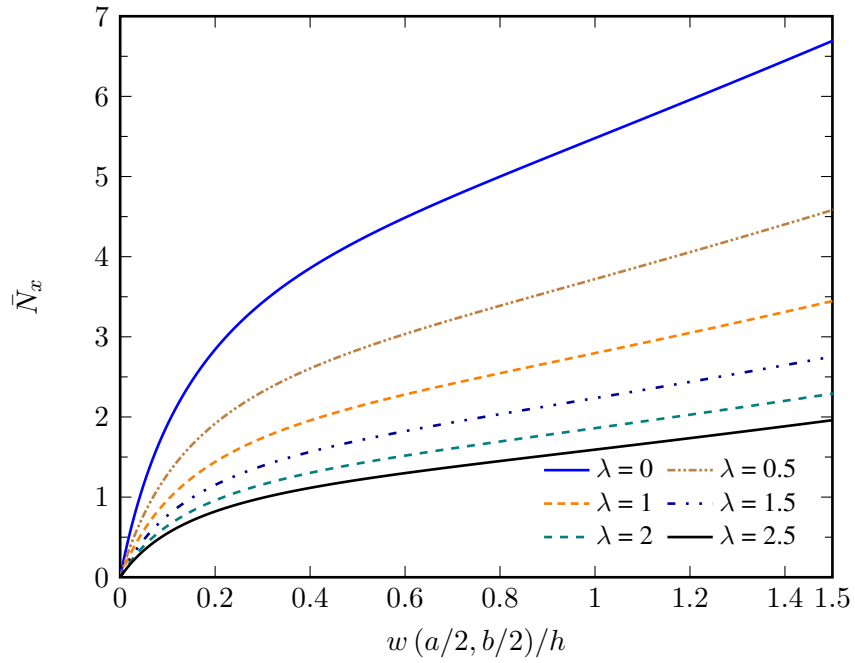


(b) SSSS2, $\kappa = 2$

Figure 5: Influence of nonlocal parameters on postbuckling paths of square FG nanoplate ($\lambda = 0, h/a = 0.05$)



(a) SSSS1, $\kappa = 0$



(b) SSSS1, $\kappa = 2$

Figure 6: Influence of ratio of compressive loads λ on postbuckling paths of square FG nanoplate ($\epsilon_0 a = 0.2$ nm, $h/a = 0.05$)

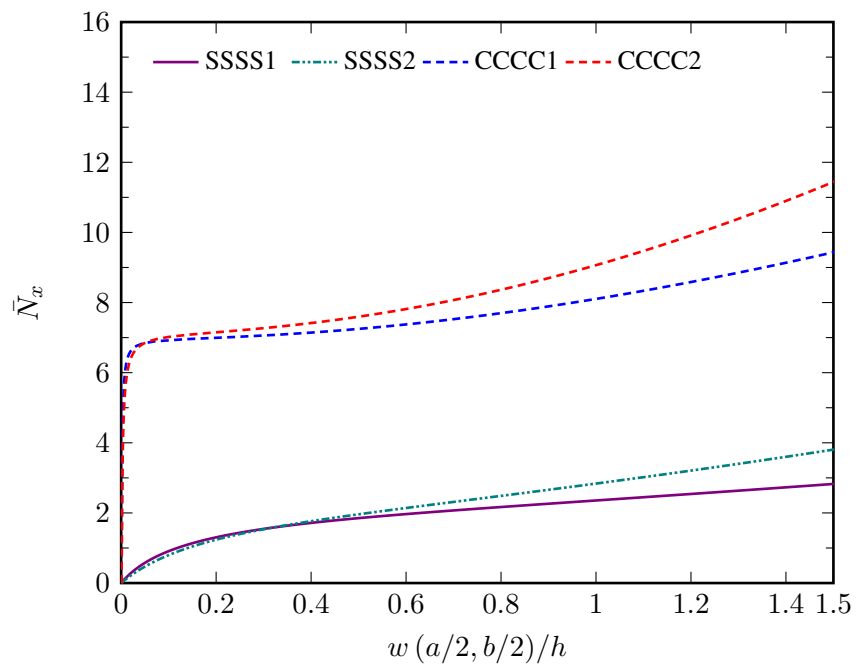


Figure 7: Influence of boundary condition on postbuckling paths of square FG nanoplate ($\lambda = 1$, $e_0 a = 0.25$ nm, $\kappa = 5$, $h/a = 0.05$)

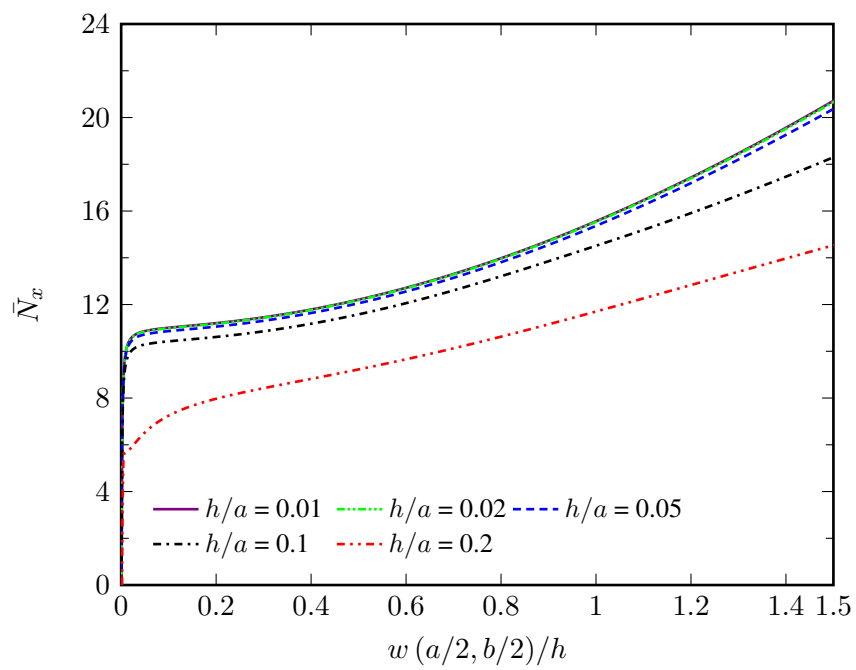
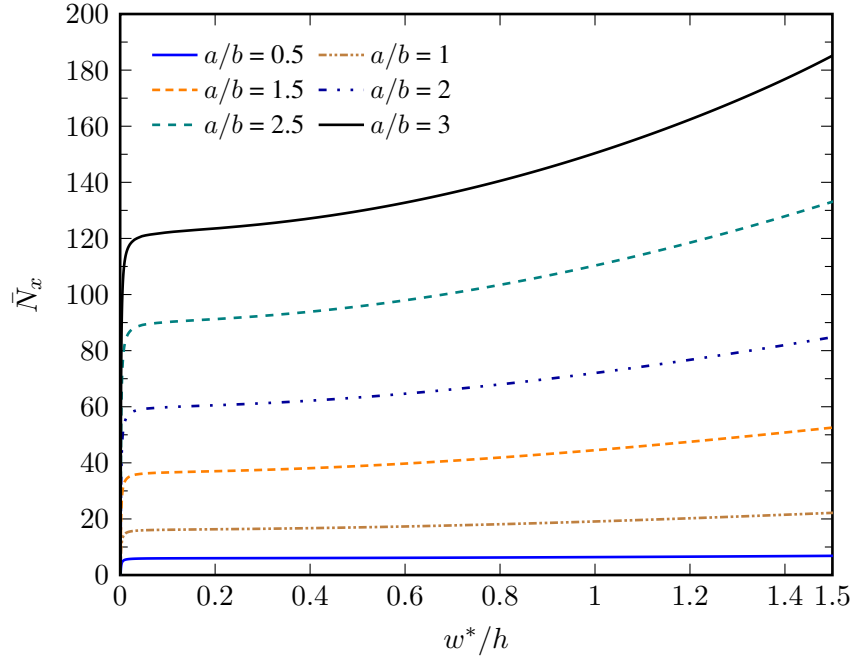
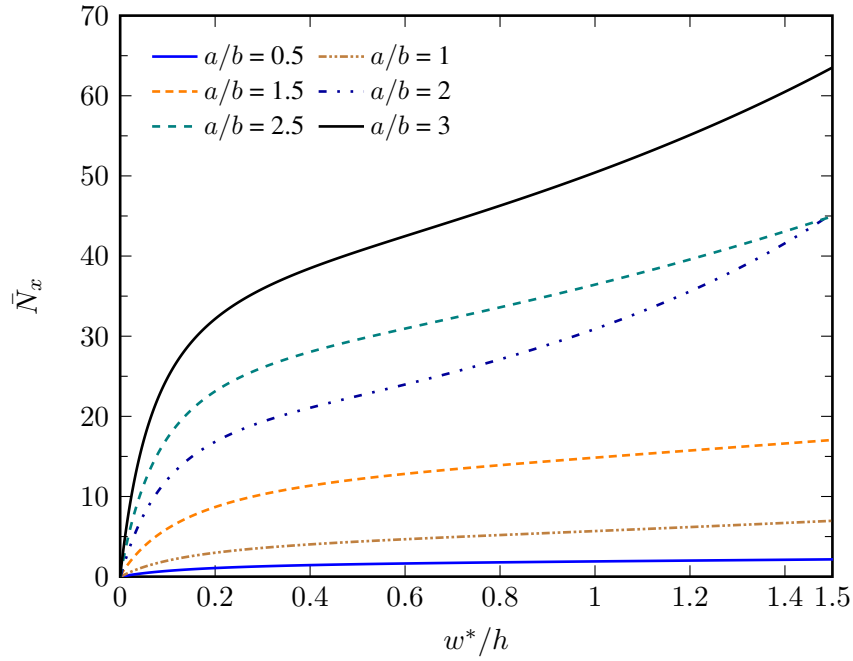


Figure 8: Influence of thickness ratio on postbuckling paths of square FG SSSS2 nanoplate ($\lambda = 1$, $e_0 a = 0.15$ nm, $\kappa = 0$, $h/a = 0.05$)



(a) SSSS1, $\kappa = 0$



(b) SSSS1, $\kappa = 2$

Figure 9: Influence of geometrical ratio (a/b) on postbuckling paths of FGM nanoplate ($\lambda = 0$, $e_0a = 0.15$ nm, $h/a = 0.05$)

$w^* = w(a/2, b/2)$ for $a/b = 0.5, 1$, $w^* = w(a/4, b/2)$ for $a/b = 1.5, 2$ and $w^* = w(a/6, b/2)$ for $a/b = 2.5, 3$

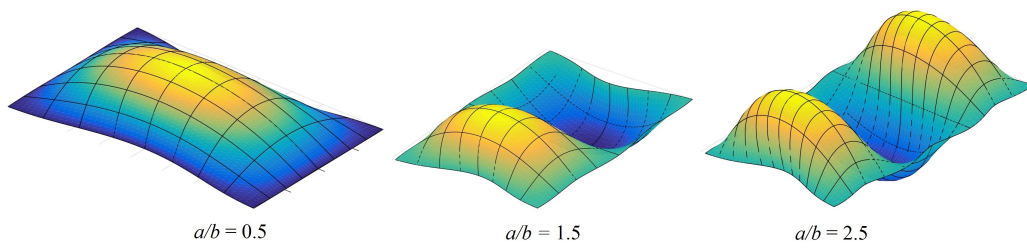


Figure 10: Illustrations of buckling deformed shapes of homogeneous ($\kappa = 0$) SSSS1 nanoplates (scale factors are used for illustration purpose)

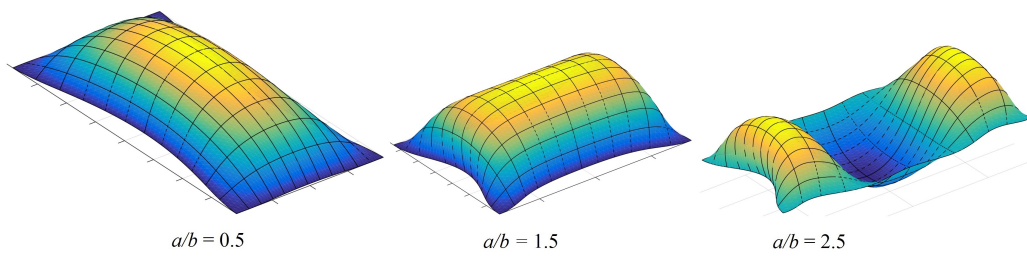


Figure 11: Illustrations of buckling deformed shapes of FG ($\kappa = 2$) SSSS1 nanoplates (scale factors are used for illustration purpose)